Acta Geologica Sinica (English Edition), 2020, 94(5): 1471–1487

Characteristics of Uranium Mineralization in Red Clastic Formations in the Southwestern Margin of the Ordos Basin

ZHANG Zilong[1], HE Feng[1], YI Longsheng[1, *], FAN Honghai[1], CAI Yuqi[1], LIU Hongxu[1], LIU Xinyang[2], CHEN Hongbin[3], JIA Cui[1] and YANG Mengjia[1]

[1] *Key Laboratory of Uranium Resource Exploration and Evaluation Technology (CNNC), Beijing Research Institute of Uranium Geology, Beijing 100029, China*

[2] *China National Uranium Corp., Beijing 100013, China*

[3] *No.203 Research Institute of CNNC, Xianyang, Shaanxi 712000, China*

Abstract: In the southwestern margin of the Ordos Basin, uranium mineralization is primarily hosted by predominantly oxidative red clastic formations in the Lower Cretaceous. The main target layers for uranium exploration are the Madongshan and Liwaxia formations of the Liupanshan Group, followed by the Jingchuan Formation of the Zhidan Group. The host rocks (medium-fine feldspar quartz sandstone), which are bleached to a light grayish white color, contain a minor organic matter component and pyrite. Uranium mineralization changes from surficial infiltration or phreatic oxidation in the upper part to interlayer oxidation in the lower part. Uranium ore bodies are mostly lenticular or tabular in shape, locally shaped like crescent rolls. Individual ore bodies are typically small and shallow. Uranium predominantly manifests as pitchblende and coffinite. Coffinite is usually short and columnar or granular in habit, whereas pitchblende occurs as an irregular colloidal covering on the surface or in fissures of ferric oxide, silicate, clay or carbonate. Secondary uranium minerals are torbernite, uranophane, and uranopilite. Minerals associated with uranium are mainly pyrite, chalcopyrite and, to a minor extent, arsenopyrite and fluorite. The associated elements are Mo, V, Se, Co, Ni, and Mn, the host sandstone being high in Cu and Ba. Overall, the red clastic formations in the southwestern margin of the Ordos Basin are characterized by 'five multiples but one low' which means multiple target layers, multiple stages of mineralization, multiple ore body shapes, multiple kinds of uranium minerals, multiple associated elements, but low organic matter. This implies an overall complex uranium metallogenic environment and mineralization process. It is recommended that future uranium exploration should take into consideration regional metallogenic conditions and mineralization features, with target layers in the wide-smooth synclinal slope being focused on. Most uranium deposits are small to medium in size, and the main type of uranium mineralization can vary by target layer.

Key words: red clastic formation, uranium mineralization, Lower Cretaceous, southwestern Ordos Basin

Citation: Zhang et al., 2020. Characteristics of Uranium Mineralization in Red Clastic Formations in the Southwestern Margin of the Ordos Basin. Acta Geologica Sinica (English Edition), 94(5): 1471–1487. DOI: 10.1111/1755-6724.14500

1 Introduction

Sandstone–type uranium deposits in China are mainly found in two kinds of clastic formations: the gray clastic formations in the Lower–Middle Jurassic Series and the red clastic formations in the Cretaceous, Paleogene or Neogene (Liu et al., 1997; Chen et al., 2003; 2011). Uranium mineralization is mainly hosted by red clastic formations interlayered with gray medium- or fine-grained clastic formations. Red clastic formations are the main uranium–producing and prospecting target layers in the Erlian and Songliao Basins of northern China, where many large and medium-sized uranium deposits have been found, such as the Qianjiadian (Luo et al., 2007; Pang et al., 2010) and Baolongshan (Xu et al., 2011) deposits in the Songliao Basin and the Nuheting and Subeng deposits (Kang, 2011) in the Erlian Basin. Several small and medium-sized uranium deposits have also been found in other basins, such as the Hongshan deposit (Li et al., 2010) in the Jiudong Basin, the Dahongshan deposit (Guo et al., 2015) in the Chaoshui Basin, the Wangjiachong deposit (Jiang et al., 2017) in the Hengyang Basin and the Guojiawan deposit (Sun, 1998; Chen et al., 2011) and the Hangjinqi Deposit (Zhang et al., 2017) in the Ordos Basin. Thick red clastic formations are widespread throughout all basins in northern China and in the red basins in southern China; therefore, studies on the characteristics of uranium mineralization in red clastic formations will expand the exploration space of sandstone–type uranium resources in China.

Uranium mineralization in red clastic rock formations in the Erlian and Songliao basins has been systematically studied, resulting in breakthroughs in uranium exploration. However, studies on uranium mineralization in the southwestern Ordos Basin are still relatively limited, in particular in terms of geological reactions, geological features and key ore-controlling factors. Such gaps in the

* Corresponding author. E-mail: roedder@126.com

© 2020 Geological Society of China

research have greatly limited uranium exploration in the Ordos Basin. On the basis of earlier work (Sun, 1998; Chen et al., 2011), we used a combination of macro- and micro-scale analyses to investigate the geological features of uranium mineralization in the Guojiawan uranium deposit. For example, we analyzed regional geological data and representative drilling results for uranium sources, structures, sandstones, oxidation zones and uranium ore bodies, which identify the main target layers and ore-controlling factors. We also analyzed mineralogy (thin section, SEM), geochemistry (major and trace elements) and stable isotopes (S) to identify the lithologies and textures of host rocks; the existence, mineral types and concentration environment of uranium; and associated minerals' assemblage and element combinations. We argue that uranium mineralization in the studied area can be characterized by 'five multiples but one low'. Moreover, we analyze metallogenic conditions, identify key regional factors that affect uranium mineralization and interpret the mechanism of uranium metallogenesis. A significant discovery is that uranium exploration in the southwestern Ordos Basin can be improved to target multiple types in multiple target layers instead of only the interlayer oxidation zone in the Madongshan Formation. This increases the prospective space in the southwestern Ordos Basin, improves the potential for uranium exploration and provides a theoretical basis for uranium prospecting in red clastic formations in the southwestern Ordos Basin.

2 Regional Geology

2.1 Regional geological settings

The present tectonic framework of the Ordos Basin was initiated by the middle Yanshan Movement, then evolved and became established in the Himalayan Movement. The basin can be divided into six second–order units: the Yimeng uplift, Weibei uplift, Jinxi flexural fold belt, Shanbei slope belt, Tianhuan depression and western thrust structural belt (Li et al., 1980; Liu et al., 1986; He et al., 2003; Deng et al., 2005; Zhang et al., 2011). The Jurassic Liupanshan uplift, which emerged as a paleo-ridge in the western basin, separates the Liupanshan Basin and the Ordos Basin. Uranium mineralization in the southwestern Ordos Basin occurs at the confluence of the southern end of the western thrust belt, the southern Tianhuan depression, the northern Weibei uplift and the southwestern Shanbei slope belt (Fig. 1).

From Longxian to Chongxin in the southwestern Ordos Basin, the NNW-striking slope belt in the basement is about 30–40 km long and has a modest dip (5°–10°). The structures in the cover were mainly influenced by the Yanshanian Movement and formed an eastward-dipping, steadily sloping belt. Therein, the Lijiahe syncline, which controls uranium mineralization in the Guojiawan deposit and its periphery, represents a pre–ore structure developed in the basement depression. After Cretaceous sedimentation, the syncline was lifted up and tilted by compression of the western fault–fold belt and Weibei uplift. This formed a broad syncline that dips gently to the basin center.

2.2 Regional stratigraphy

In the southwestern Ordos Basin, the Meso–Cenozoic cover is composed of the Yanchang Formation (Zhu, et al., 2019) of the Upper Triassic, Jurassic, Lower Cretaceous, Oligocene, Pliocene and Quaternary (Fig. 2). In the southwestern part of the study area, the Lower Cretaceous mainly consists of the Liupanshan Group, which from bottom to top comprises the Sanqiao (K_1s), Heshangpu (K_1hs), Liwaxia (K_1g), Madongshan (K_1m) and Naijiahe (K_1n) formations (Hao, 1986; Song, 1993). These strata were conformably deposited, with a total thickness of 1,500 m. Towards the center of the basin, the Zhidan Group is exposed in the study area, from bottom to top comprising the Yijun (K_1y), Luohe (K_1l), Huachi (K_1ch)–Huanhe (K_1h), Luohandong (K_1lh) and Jingchuan (K_1j) formations (Hao, 1986; Yang, 2006), with a total thickness of 700–1100 m. There are two formations (Sanqiao and Heshangpu) in the lower section of the Liupanshan Group and three formations (Liwaxia, Madongshan, and Naijiahe) in the upper section, that correspond approximately to the Luohandong and Jingchuan formations in the Zhidan Group, respectively (Fig. 3). The ore-hosting target layers are mainly the Madongshan and Liwaxia formations of the Liupanshan Group, then the Jingchuan Formation of the Zhidan Group. Some uranium has also been found in recent years in the Heshangpu Formation of the Liupanshan Group.

3 Sampling and Analytical Methods

3.1 Sampling

Given the characteristics of uranium mineralization of the Lower Cretaceous in this area, fresh uraniferous or redox zone samples were collected from the Madongshan and Liwaxia formations through drilling in the Lijiahe syncline. A portable X-fluorescence instrument was used to semi-quantitatively determine the uranium content of core samples, and samples with uranium greater than 100 ppm were selected for study. The redox zone samples were collected from different lithologies after delineation of strong oxidation, weak oxidation, and redox-transition zones in drill hole profiles. Sample analyses, which included major element analyses, trace element analyses, scanning electron microscopy and thin–section petrography, were conducted at the Analytical Laboratory of the Beijing Research Institute of Uranium Geology.

3.2 Analytical methods

Weathered surfaces were cut and removed, the samples then being ground to less than 200 mesh with agate mortar.

We analyzed the major elements using an X-ray fluorescence spectrometer (Philips PW2404) with an analytical precision in excess of 1%. Details of the specific process are as Norrish and Hutton (1969).

Trace element analyses of the whole rock were conducted on a Finnigan MAT Element I ICP-MS at the Analytical Laboratory of the Beijing Research Institute of Uranium Geology in Beijing, China. Samples were digested with acid, the trace elements analyzed including Li, Be, Sc, V, Cr, Co, Ni, Cu, Zn, Ga, Rb, Sr, U, Pb, Y,

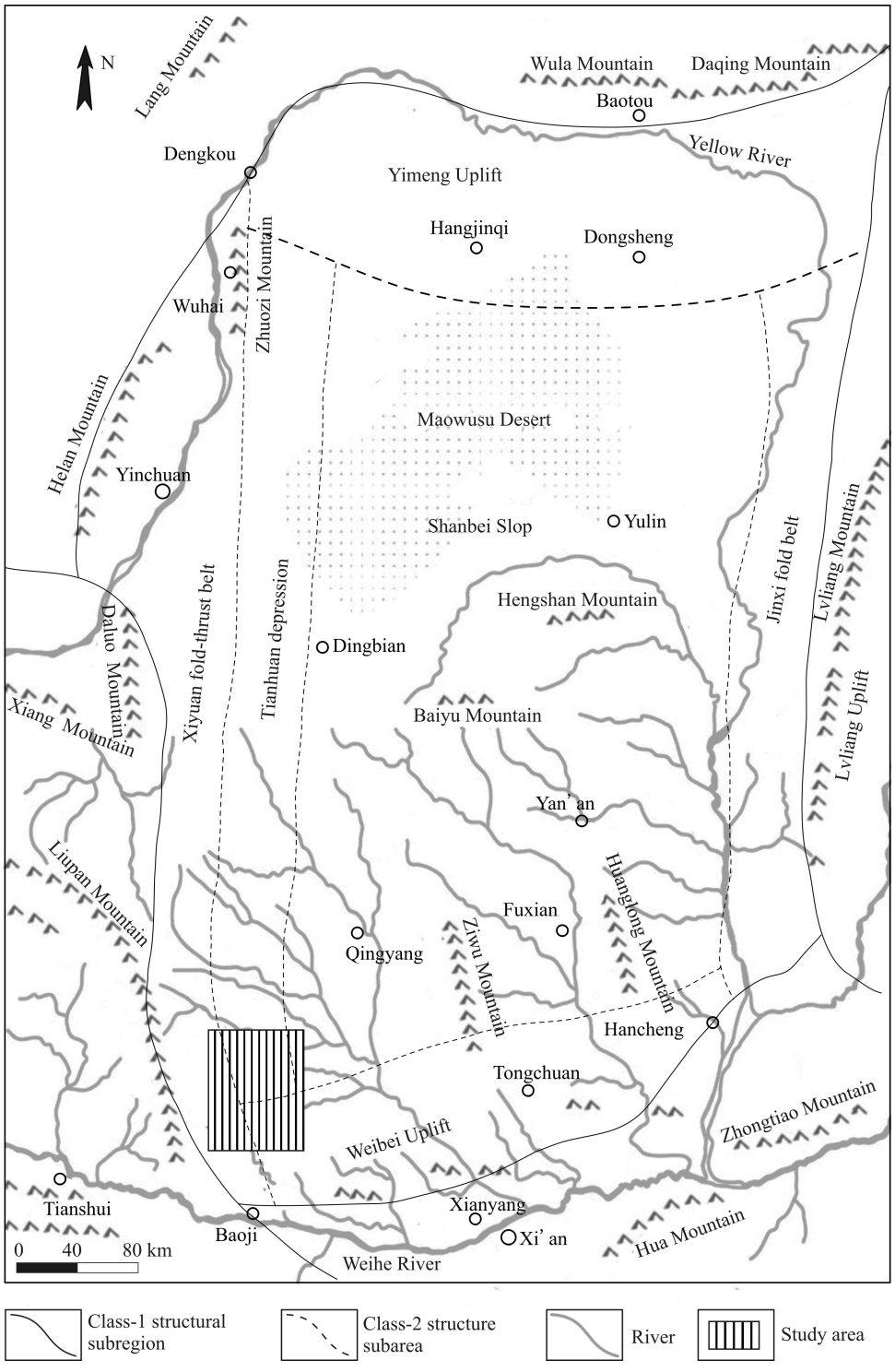


Fig. 1. Geotectonic map of the Ordos Basin, showing the location of the study area.

REE, W, Re, Tl, Bi, Th, Zr and Hf. The analytical and QAQC procedures were as follows. (1) Each sample was ground separately for chemical preprocessing. Samples were ground to less than 200 mesh, and a quarter of each sample powder was set aside for assaying. (2) The Teflon bomb was checked for background radiation before it was used in the chemical assay process. Duplicate samples and CRMs (GBW07106 [GSR-4] quartz sandstone and GBW07725 [GSR-16] uranium–bearing sandstone) were inserted into the samples to be assayed at an insertion rate of 20% in total. (3) Each sample was chemically processed according to the standard flow regulated by the National Code 'Chemical Analysis Method of Silicate Rocks Section 30: Assay of 44 Elements' before being assayed

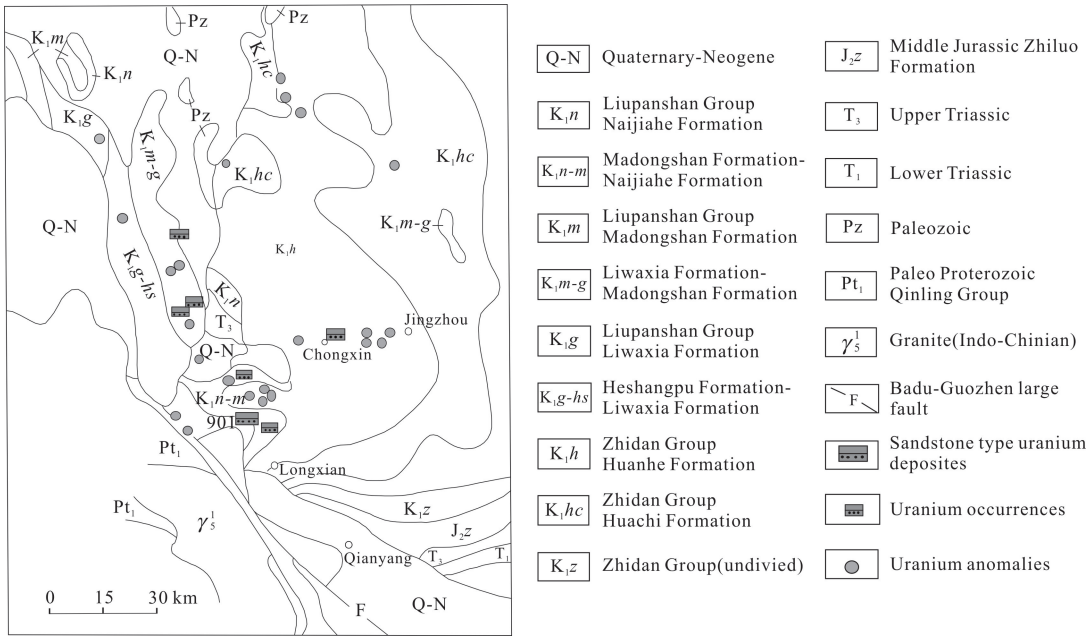


Fig. 2. Geological sketch of the southwestern Ordos Basin, showing uranium deposits, occurrences and anomalies (after Sun Gui et al., 1998).

by high–resolution ICP-MS. The quality of the assay process was controlled by internal calibration and instrument parameter adjusting. The chemical assay qualified only if the relative standard variation between duplicate samples was less than 5% and the accuracy of the CRM was greater than 99.9%.

A field emission scanning electron microscope (Nova Nano SEM 450-type) was used to identify the minerals, based on instructions provided in JY/T 010-1996 'General Rules for Analytical Scanning Electron Microscopy' and GB/T 17361-2013 'Microbeam Analyses of Authigenic Clay Minerals in Sedimentary Rocks by Scanning Electron Microscope and Energy Dispersive Method.'

Uranium isotopes were analyzed on an Isoprobe_T Thermal Ionization MS with triple bands of Ta–Re–Ta, lead isotopes being analyzed on a Phoenix Thermal Ionization MS with a single band of Re. The phosphoric acid–silica gel method was used. TIMS analyses were conducted in the static multi–receiving mode with a Faradic Cup. One CRM NBS981 was added to every batch of Pb samples for isotopic analysis, and one UTB500 was inserted into every batch of U samples for isotopic analysis; 10% duplicate samples were inserted per batch to monitor the quality of the data. Acceptable precision for CRM analyses is $^{208}Pb/^{204}Pb$ = 36.690 ± 0.004, $^{207}Pb/^{204}Pb$ = 15.489 ± 0.001, and $^{206}Pb/^{204}Pb$ = 16.936 ± 0.002 (for NBS9810) and $^{235}U/^{238}U$ = 1.022220 ± 0.00015 (for UTB500).

Sulfur isotope analyses were conducted on a Flash 2000 element analyzer and a Delta v Plus stable isotopic gas MS. Each sample of pyrite or chalcopyrite was taken to have a total sulfur content of 54 ± 6 μg and wrapped in a tin bag. The ionic flow intensity of the reference gas was set at 3V, and the Conflo IV-He gas-loading pressure was 1.01×10^5 Pa. In the EA system, the He flow rate was 100 mL/min and the O flow rate was 150 mL/min. The oxygen loading time was 3 s, and the temperature of the reaction stove was 1020° C. The temperature of the chromatographic pole was 90°C. Results of the analyses were standardized with CDT and recorded as δ^{34}SV–CDT. The precision of the analyses was better than ±0.2‰. The CRMs of sulfide are IAEA-S-1, IAEA-S-2 and IAEA-S-3, of which the δ^{34}S were −0.21 ± 0.13‰, 22.53 ± 0.14‰ and –32.35 ± 0.18‰, respectively.

Geokit software, developed by Lu (2004), was used to draw the charts.

4 Uranium Mineralization

4.1 Ore bodies

Uranium mineralization in the southwestern Ordos Basin mainly lies on both wings of the Lijiahe syncline (Fig. 4), the uranium mineralization belt being about 20 km long and primarily being constrained by the Madongshan and Liwaxia formations of the Lower Cretaceous.

Uranium mineralization in the southwestern Ordos Basin mainly lies on both wings of the Lijiahe syncline (Fig. 4). The uranium mineralization belt is about 20 km long and is mainly constrained by the Madongshan and Liwaxia Formations of the Lower Cretaceous.

Uranium mineralization in the Madongshan Formation is small in scale and is mainly represented by the Guojiawan deposit over an area of about 4.5 km^2. Uranium mineralization mainly occurs where the purple-red sand body and grayish green/light gray sand body make contact in the middle–upper Madongshan Formation. It is mainly related to interlayer oxidation, with roll-shaped ore bodies being controlled by the front of the oxidation zone (Fig. 5). The ore bodies are generally

Liupanshan Group						Upper Zhidan Group					
Stratum	Histogram	Thickness (m)	Sedimentary environment	Uranium mineralization	Lithology characters	Stratum	Histogram	Thickness (m)	Sedimentary environment	Uranium mineralization	Lithology characters
Naijiahe Fm. (K_1n)		0 – 144	Lake facies		Top:purplilsh red mudstone Bottom: steel gray mudstone 	Jingchuan Fm. (K_1j)		270 – 540	Shore shallow lacustrine—fluvial facies	Jiaojiahui mineral spot Two industrial hole	Purplish red, purplish brown mudstone, sandy mudstone with thin fine sandstone and marlite, near basin's west edge is mainly sandstone with mudstone 
Madongshan Fm. (K_1m)		0 – 271	River facies	Guojiawan Uranium Deposits	Top: purplish red sandy mudstone, middle: yellow, light red coarse sandstone Bottom: purplish red mudstone 						
Liwaxia Fm. (K_1g)		80 – 201	River and lake facies	Iindustrial Hole	Top: steel gray shale Middle and bottom: mid-thick purplish red mudstone 						
Heshangpu Fm. (K_1hs)		130 – 208	River and lake facies		Top: interbedding of sandstone and mudstone Bottom: mid-thick coarse sandstone 	Luohandong Fm. (K_1lh)		100 – 175	Fluvial—shore shallow lacustrine facies		Top: brownish red, brownish yellow fine sandstone, middle-coarse sandstone with thin dark purple mudstone Bottom: middle-thick glutenite 
Sanqiao Fm. (K_1s)		20 – 850	Piedmont pluvial facies		Purple, brownish red glutenite 						

Fig. 3. Comprehensive stratigraphic column of the southwestern Ordos Basin.

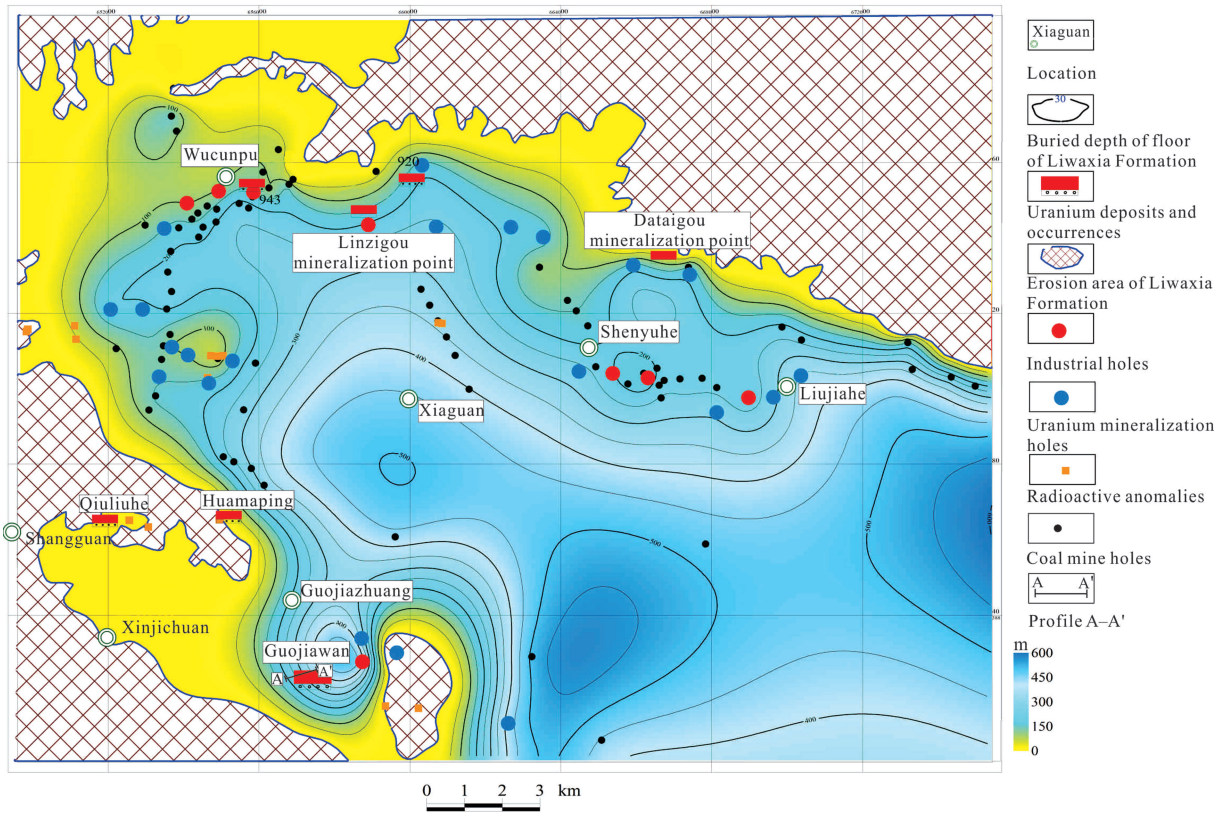


Fig. 4. Location of uranium mineralization in the Lijiahe syncline, southwestern Ordos Basin.

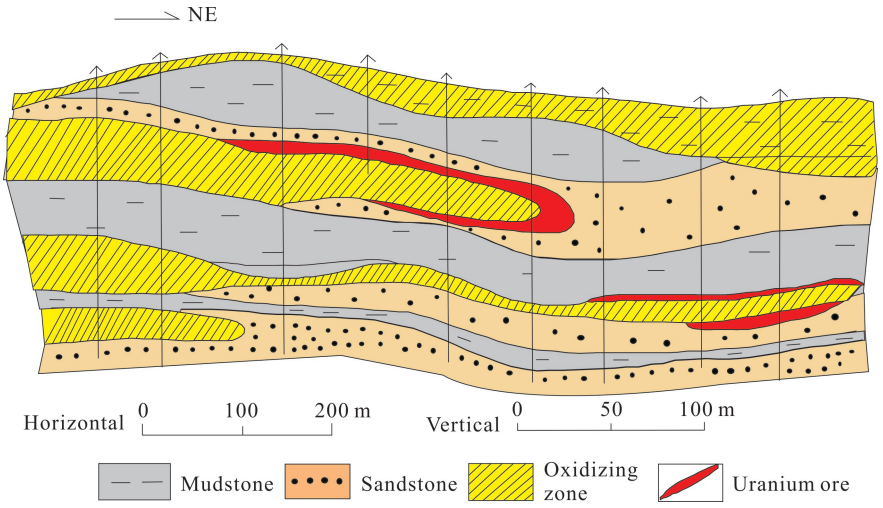


Fig. 5. Profile A–A' in section 1431 in the Guojiawan deposit (Sun Gui et al., 1998).

100–200 m in length, with a maximum length of 400 m, generally less than 2m thick, with a maximum thickness of 3.15m and an average thickness of 1.16 m. The average grade is 0.046% U and the buried depth is 50–200 m (Sun, 1989). In addition, the uppermost ore layer was lifted up over the base erosion level by subsequent structural movement and has been damaged by intensive undercutting by present-day rivers.

Uranium mineralization in the Liwaxia Formation extends widely within 5 km of the erosion edge of the Liwaxia Formation, in both wings of the Lijiahe syncline. Uranium mineralization mainly occurs in the light grayish white fine- to-medium sandstones that are interbedded by the purple-red mudstone of the Liwaxia Formation. The uranium ore bodies are predominantly lentoid (Fig. 6), usually ranging in thickness from 1.60 to 2.50 m; the average grade is 0.062%, the buried depth generally being in the range 6.6–154.5 m. The major ore body is located at a depth of 50–100m, beneath the unconformity lying between the Liwaxia Formation and the Neogene.

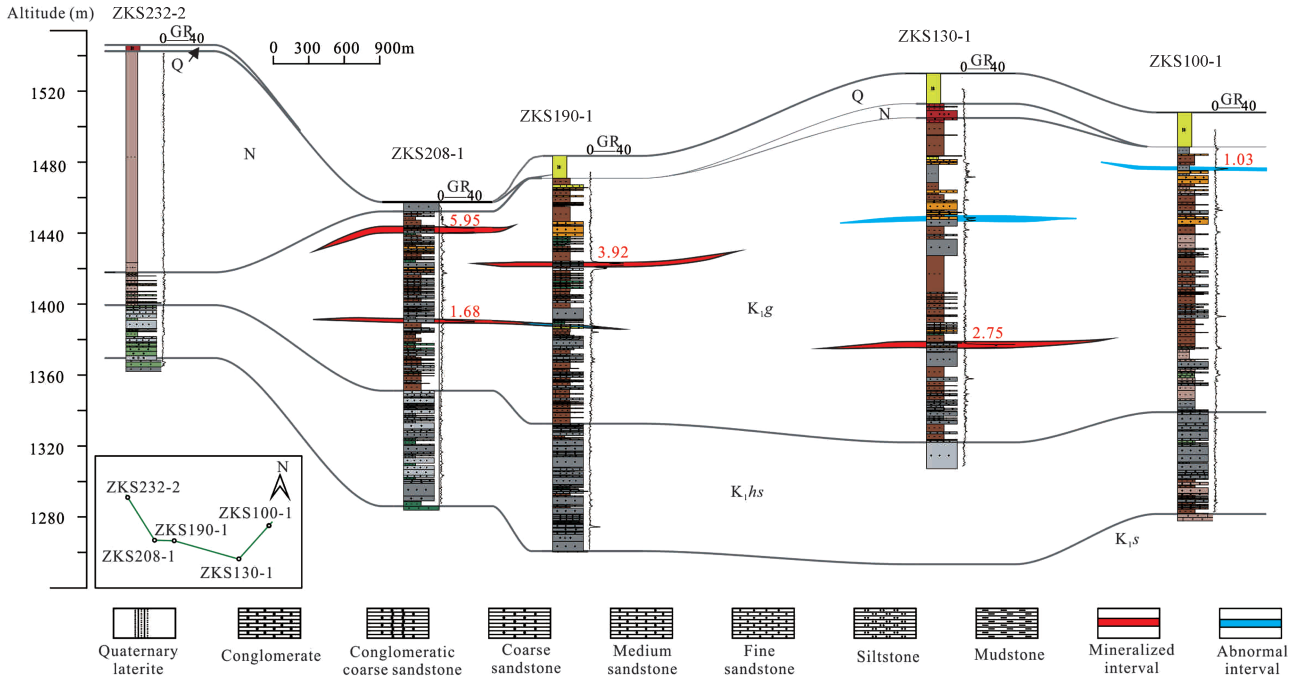


Fig. 6. Location of uranium ore bodies in a profile of the Shenyuhe section in the Liwaxia Formation.

4.2 Oxidation zone

Three confined aquifers occur in the Madongshan Formation, each containing a superimposition of multiple stages of the interlayer oxidation zones, which are large and extend distally. Each individual oxidation zone is generally 20–40 m thick (maximum = 50 m), several kilometers wide, extending like a tongue or bed locally, separated and reunited. The oxidation zone is clearly marked with alteration. Along the dipping direction of the zone, the sandstone oxidation decreases and the rocks darken with more organic matter and pyrites. In the strong oxidation zone, the rocks are yellow to yellow-brown and locally purple-red, with ferrous oxide and ferrous–manganese hydroxide distributed along the bedding, the ratio of Fe^{3+} to Fe^{2+} being as high as 16.10. In the weakly oxidised zone, the rocks are grayish yellow, and the ratio of Fe^{3+} to Fe^{2+} being greater than 1.28. Uranium is significantly enriched with a concentration of 0.025%–0.030% U. In the redox transitional zone, the rocks are grayish green to green-gray and contain significant organic matter, carbon fragments and pyrite, the ratio of Fe^{3+} to Fe^{2+} being less than 1. Uranium concentrations can reach 0.1% U or more (Zhang et al., 2011).

Roll–shaped uranium ore bodies occur around the front of the oxidation zone and lie in the transition between the grayish green sandstone and the gray sandstone. The grayish green color is mainly due to conifer–shaped chlorite coated on sand grains (Fig. 7a), similar to the Dongsheng uranium ore field, where the ore–bearing sandstone is also green (Li et al., 2007; Yi et al., 2015; Li et al., 2017). In the oxidation zone, the sandstone demonstrates strong epigenetic alteration with oxidation, such as predominant limonitization, as well as hydromicazation and chloritization of biotite, feldspar and magmatic rock detritus.

The oxidation zone in the Liwaxia Formation extends to about 20 km in length and 5 km width from both wings towards the core of the Lijiahe syncline, the thickness of an individual layer generally being less than 2m. The oxidation alteration can be divided into the primary alteration zone, the epigenetic alteration zone and the late alteration zone, according to geochemical features. In the primary zone, brownish red or brick–red oxidation alteration occurs, with a few gray mudstones locally; the total Fe content is 2.83%–4.44% (average = 3.77%), organic carbon is 0.04%–0.12% (average = 0.07%), total sulfur is 0.015%–0.047% (average = 0.03%), uranium is 3.4–4.8 ppm (average = 3.77 ppm), CO_2 content is 1.28%–6.26% (average = 4.18%). In the epigenetic zone, the fading of the sandstone and a few mudstones to gray, grayish white, or grayish green is mainly caused by reduction alteration; the total Fe content is 1.20%–4.70% (average = 2.20%), organic carbon is 0.02%–0.22% (average = 0.056%), total sulfur is 0.035%–2.81% (average = 0.70%), uranium is 2.0–15.8 ppm (average = 7.30 ppm), CO_2 is 3.53%–8.64% (average = 5.42%). Uranium is mainly hosted in the thin beds of grayish white fine sandstone and siltstone. The content of reductive materials is relatively high in this zone, the original sandstone being altered and bleached to a grayish white or grayish green color, with the formation of alteration minerals such as carbonate, clay and chlorite. In the late alteration zone, brownish yellow or purple-red oxidation alteration appears in bands; the total Fe content is 0.77%–2.03% (average = 1.17%), organic carbon is 0.01%–0.04% (average = 0.03%), total sulfur is 0.011%–0.62% (average = 0.12%), uranium is 1.5–9.9 ppm (average = 4.00 ppm), CO_2 is 1.46%–13.52% (average = 4.97%; Table 1).

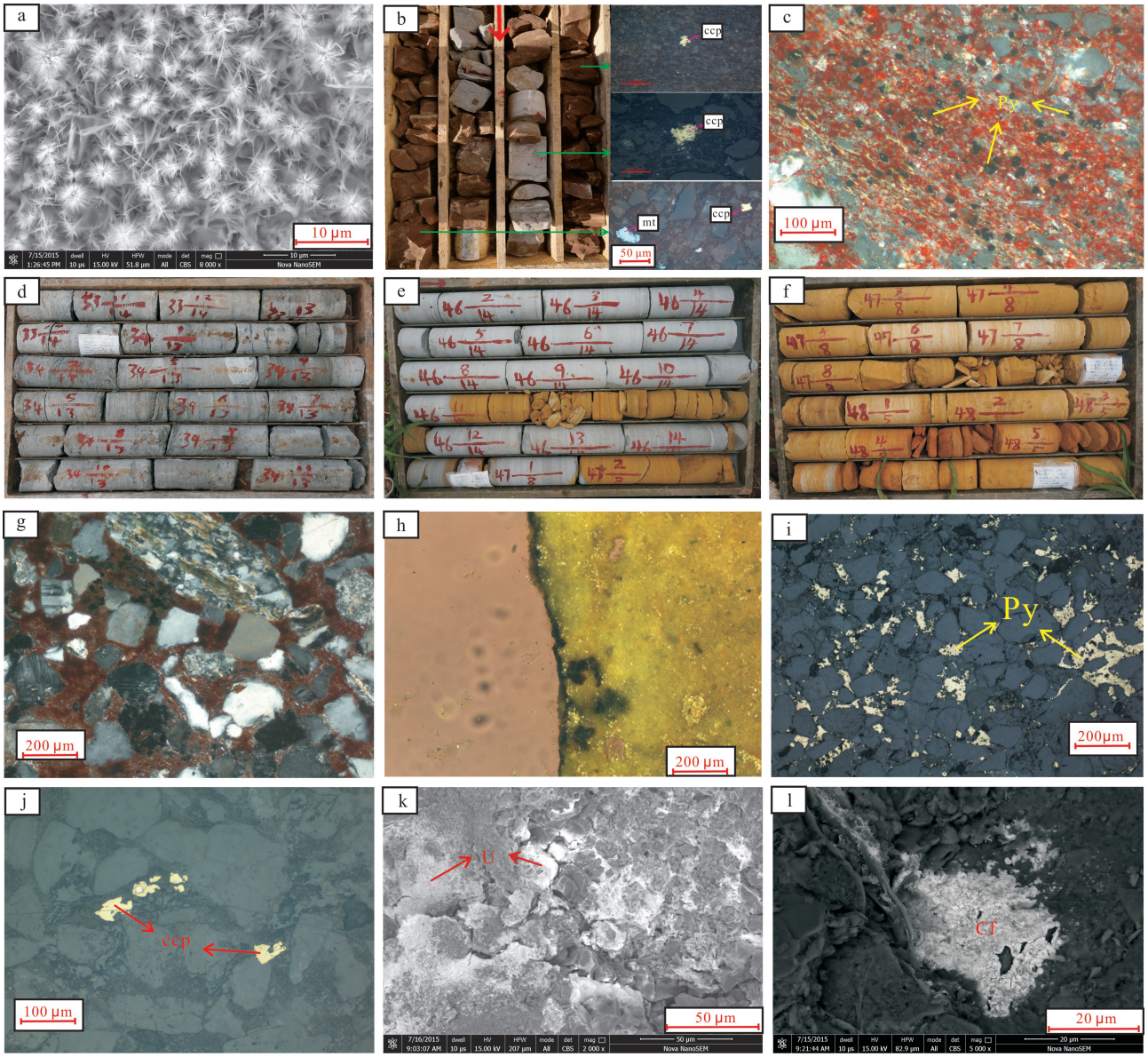


Fig. 7. Alteration and mineralogical assemblages of uranium target layers in the southwestern Ordos Basin.
(a) Coniferous chlorite in gray–green sands (ZKG7–1, 229 m); (b) Purple–red mudstone interbedded with gray–white ore–bearing sandstone in the Liwaxia Formation, chalcopyrite and pyrite occurring in various lithological sections (ZKS73–1); (c) Abundant fine pyrite in purple–red sandstone (10×20, crossed polarized light, ZKS190–1, 60.0 m); (d) Thick syngenetic gray sands of the Heshangpu Formation, which contain pyrite and minor carbonic clasts (ZKM20–5); (e) Interlayer oxidation zone of the Heshangpu Formation (ZKX0–1); (f) Thick yellow sands in the interlayer oxidation zone of the Heshangpu Formation (ZKX0–1); (g) Poorly-sorted clasts, porously basally cemented (10×10, crossed polarized light, ZKS73–1, 135.4 m); (h) Organic veins filling in mudstone fissures (10×10, crossed polarized light, ZKS130–1, 37.15 m); (i) Abundant disseminated fine pyrite associated with pitchblende in rocks (10×10, crossed polarized light, ZKS130–1, 154.6 m); (j) Micro chalcopyrite in rocks (10 × 20, crossed polarized light, ZKS190–1, 60.35 m); (k) Abundant granular or nebular uranium minerals on surface or in fissures of silicate crystals (ZKS73–1, 135 m); (l) Fine coffinite assemblages in clay minerals (ZKS19–1, 101 m).

Powdered limonite infilling is superposed on the light gray altered sandstone in the late alteration zone, xenomorphic granular pyrite and chalcopyrite being observable. Chalcopyrite, pyrite and magnetite can be found in all alteration zones (Fig. 7b–c).

Although no uranium ore body has been found in the Heshangpu Formation, syngenetic gray sandstones occur in this layer. These thick and extensive sandstones contain much pyrite and minor organic matter (Fig. 7d). The epigenetic oxidation alteration in these sands is strong and interlayer oxidation zones are developed (Fig. 7e–f).

4.3 Uranium ores and mineralogy

Uranium ores in the Madongshan Formation are hosted in fine to medium–coarse feldspar quartz sandstones and a few feldspar quartz graywackes containing 70%–80% quartz, 5%–13% feldspar, 2%–8% detritus and a little biotite. The clasts are commonly angular or subangular, the rocks of low maturity. There are many pyrites and a few types of organic matter that locally form gray bands in the ores. The ores are mainly cemented by argillaceous matter, or locally by calcareous and ferrous matter, being highly permeable. Most of the feldspar and magmatic rock

Table 1 The geochemical characteristics of sandstone in different alteration zones in the Liwaxia Formation

Alteration zones	Sample ID	ΣFe (%)	orgC (%)	Σ S(%)	CO_2 (%)	U (ppm)
Brownish red or brick–red oxidized sandstone in the primary alteration zone	G16-1	4.16	0.09	0.026	5.38	3.5
	G16-5	3.90	0.04	0.037	6.26	4.8
	G16-7	4.44	0.12	0.047	2.67	3.4
	G16-9	3.50	0.04	0.025	5.30	3.4
	G16-19	2.83	0.04	0.015	1.28	3.8
Average		3.77	0.07	0.03	4.18	3.77
Grey, grayish white, or grayish green altered sandstone in the epigenic alteration zone	G16-25	1.26	0.04	1.28	4.97	8.6
	G16-26	2.22	0.03	0.35	6.89	4.0
	G16-27	1.86	0.04	0.065	3.74	7.2
	G16-28	1.69	0.02	0.039	6.07	2.0
	G16-10	1.92	0.03	0.035	4.12	3.2
	G16-11	4.70	0.04	2.81	6.90	6.8
	G16-6	1.20	0.04	0.37	5.35	7.5
	G16-3	3.20	0.22	0.76	3.96	15.8
	G16-24	1.39	0.07	1.06	8.64	11.3
	ER16-3	2.56	0.03	0.25	3.53	6.6
Average		2.20	0.06	0.70	5.42	7.30
Brownish yellow or purple-red oxidized sandstone in the late alteration zone	G16-2	1.39	0.01	0.041	1.77	3.0
	G16-4	0.77	0.02	0.011	1.47	3.2
	ER16-5	0.80	0.03	0.62	13.52	3.3
	G16-20	0.76	0.04	0.012	3.80	1.5
	G16-21	1.44	0.03	0.030	1.46	3.1
	G16-22	0.98	0.03	0.055	7.92	4.1
	G16-23	2.03	0.03	0.042	4.88	9.9
Average		1.17	0.03	0.12	4.97	4.0

Notes: Samples were analyzed in the Analytical Laboratory of the Beijing Research Institute of Uranium Geology.

fragments have been altered to hydromica, most of the biotite has been altered to chlorite. The uranium mineral is predominantly pitchblende occurring as micro–fine grains in ferroxide and clay cements (Zhang et al., 2011). Secondary uranium minerals such as torbernite, carnotite, uranotile, and uranopilite can be found (Chen et al., 2011) on the ground and in the oxidation zone. Minor uranium is adsorbed and disseminated in the clay or organic matter between the clay beds.

Uranium ores in the Liwaxia Formation are hosted in medium–fine (feldspar) debris sandstone and graywacke containing 32%–40% quartz, 25%–30% feldspar and 3%–25% debris. They are complex and comprise magmatic, sedimentary and metamorphic rock fragments. The sandstone clasts are subangular or subround and poorly sorted, the rocks being of low compositional and structural maturity (Fig. 7g). Organic veinlets or disseminated organics occur in the ores (Fig. 7h). Many pyrites and chalcopyrites (Fig. 7i–j), predominantly present as fine or micro–grains, are observable in the ores, as are covellite, marcasite, magnetite and ilmenite. The sandstone has mainly undergone consolidation, cementation and dissolution. The cementation in the ores consists primarily of pore–based cementation by calcareous and ferrous materials (Fig. 7g) and contact cementation in a few cases. Permeability is medium to poor. Uranium is mainly adsorbed or occurs in uranium minerals, predominantly coffinite and pitchblende. The uranium minerals mainly cover the crystal surface or fill the fissures of ferrous oxide, silicate, clay and carbonate minerals (Fig. 7k, l). The distribution of coffinite is different from that of pitchblende in each horizontal oxidation subzone. Coffinite mainly occurs in light grayish white alteration zones interlayered with purple-red mudstone bands. Coffinite occurs either as individual short–columnar crystals or in a spherical assemblage of long–columnar crystals, with short–columnar coffinite commonly arising on the spherical assemblages (Fig. 8). Pitchblende mainly occurs in gray sand bodies that are in contact with grayish white sand bodies. Pitchblende fills in the pores of sandstone in the form of irregular assemblages or colloids. The boundary between pitchblende crystals is not clear (Fig. 9). Where pitchblende occurs together with coffinite, the short–columnar coffinite usually grows on the surface of the irregular colloidal pitchblende (Fig. 10), which indicates that the short–columnar coffinite formed later than the pitchblende.

4.4 Sulfide and sulfur isotopes

There are many pyrites and chalcopyrites in the Liwaxia and Madongshan formations of the Lower Cretaceous. The pyrites mainly occur in the altered sandstone that is bleached to grayish white or light gray. The chalcopyrites can be found in all alteration zones, but mostly in the light gray alteration zone. The thin sections show organic matter, pyrite, pitchblende, coffinite, calcite and chalcopyrite (Fig. 11) in the ore–hosting light sandstone of the Liwaxia Formation. Therein, organic matter fills in the gaps between sandstone clasts in the form of spots. The organic matter is surrounded by colloidal pyrite with pitchblende and, moving to the outside, micro-grained coffinite assemblages, then coffinite and calcite, and finally chalcopyrite. $\delta^{34}S$ values of pyrite differ significantly from those of chalcopyrite, although both minerals occur together with uranium minerals in the ores or the surrounding rocks of the ores. In pyrite, $\delta^{34}S$ ranges from 8.3‰ to −21.4‰ (average = −8.9‰; Table 2). In chalcopyrite, $\delta^{34}S$ ranges from 4.5‰ to 11.3‰ (average = 7.1‰).

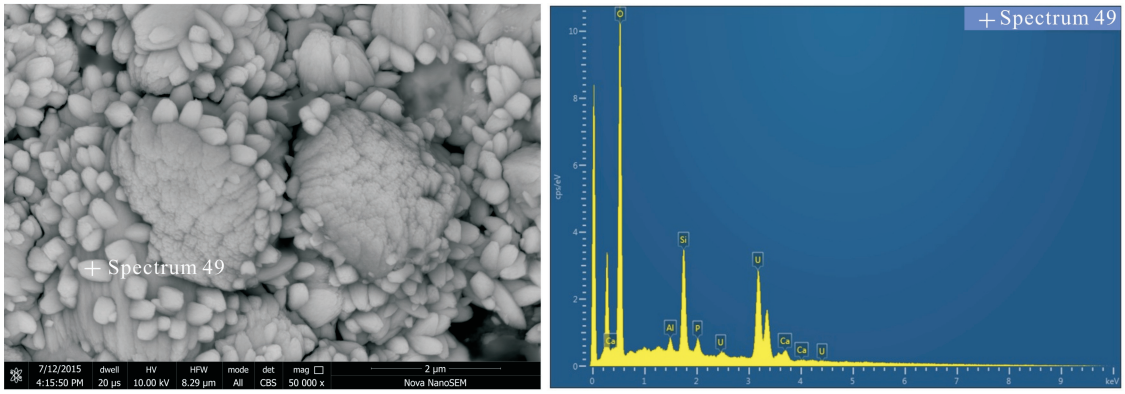


Fig. 8. Separate short–columnar coffinite and a spherical assemblage of long–columnar coffinite, Liwaxia Formation (at 62m depth of drill hole ZKS190–1).

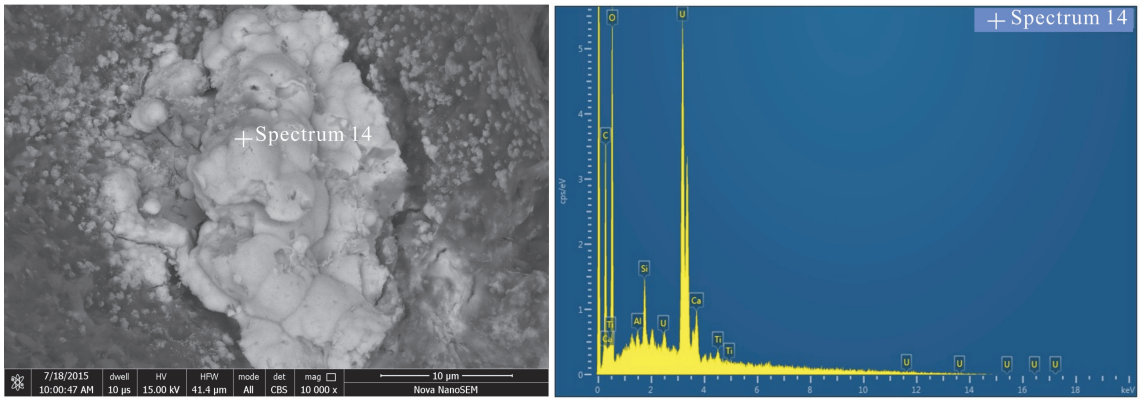


Fig. 9. Colloidal pitchblende, Liwaxia Formation (at 17.3m depth of drill hole ZKS208–1).

Table 2 Sulfur isotopes of pyrite and chalcopyrite in the uranium target layer in the southwestern Ordos Basin

Sequence No.	Sample code	Lithology	Formation	Drill hole ID	Tested mineral	$\delta^{34}S_{V-CDT}$	2SE	Position
1	D15E-10-2	Gray fine sandstone	Liwaxia	\	Pyrite	−20.9	0.07	Shenyuhe
2	D15E-10-2	Gray fine sandstone	Liwaxia	\	Pyrite	−21.4	0.10	(Niuposi ore
3	D15E-10-2	Gray fine sandstone	Liwaxia	\	Chalcopyrite	6.5	0.09	occurrence)
4	ZKS208-1-1	Gray fine sandstone with red–purple bands	Liwaxia	ZKS208-1	Pyrite	−1.0	0.22	
5	ZKS208-1-2	Gray fine sandstone with red–purple bands	Liwaxia	ZKS208-1	Pyrite	−8.3	0.16	Shenyuhe
6	ZKS208-1-1	Gray fine sandstone with red–purple bands	Liwaxia	ZKS208-1	Chalcopyrite	4.5	0.19	(ore)
7	ZKS208-1-2	Gray fine sandstone with red–purple bands	Liwaxia	ZKS208-1	Chalcopyrite	11.3	0.13	
8	ZKS130-1-5	Celadon fine sandstone	Liwaxia	ZKS130-1	Pyrite	8.3	0.09	Shenyuhe
9	ZKS130-1-5	Celadon fine sandstone	Liwaxia	ZKS130-1	Chalcopyrite	5.8	0.15	
10	ZKG7-1-18	Celadon fine sandstone	Madongshan	ZKG7-1	Pyrite	−10.0	0.08	Guojiawan

Notes: Samples were analyzed in the Analytical Laboratory of the Beijing Research Institute of Uranium Geology.

Table 3 U–Pb isotopic analysis of the Liwaxia Formation of the Lower Cretaceous in the southwestern Ordos Basin

Sequence No.	Sample code	Lithology	U (ppm)	Pb (ppm)	Results of isotopic analysis		
					$^{238}U/^{204}Pb$	$^{206}Pb/^{204}Pb$	Std err
1	ZKS-1-13	Grey fine sandstone	232	24.9	684	28.87	0.002
2	ZKS-1-15	Light yellow fine sandstone	1040	26.4	3586	47.23	0.003
3	ZKS-1-16	Light grey medium sandstone	368	17.7	962	30.06	0.003
4	ZKS-1-18	Grayish white fine sandstone	389	18.1	2530	40.32	0.003
5	ZKS-1-19	Light grey medium sandstone	506	20.3	1103	31.18	0.003

Laboratory: Analytical Laboratory of the Beijing Research Institute of Uranium Geology

4.5 Ages of uranium mineralization

The metallogenic age of the Guojiawan uranium deposit is 98 Ma (Chen et al., 2011), as documented in Uranium Geology in Northwestern China (Zhang et al., 2014). Uranium mineralization is mainly related to interlayer oxidation in the O–U-bearing paleo-aquifer at the early stage of the Late Cretaceous Epoch. We obtained a metallogenic age of 39.6 ± 2.9 Ma (Fig. 12, Table 3) according to whole-rock isochronic U-Pb isotopic dating of uranium ores from the Liwaxia Formation. Uranium mineralization in the study area mainly occurred in the Eocene of the Paleogene. Uranium mineralization

occurred significantly later in the Liwaxia Formation than in the Madongshan Formation.

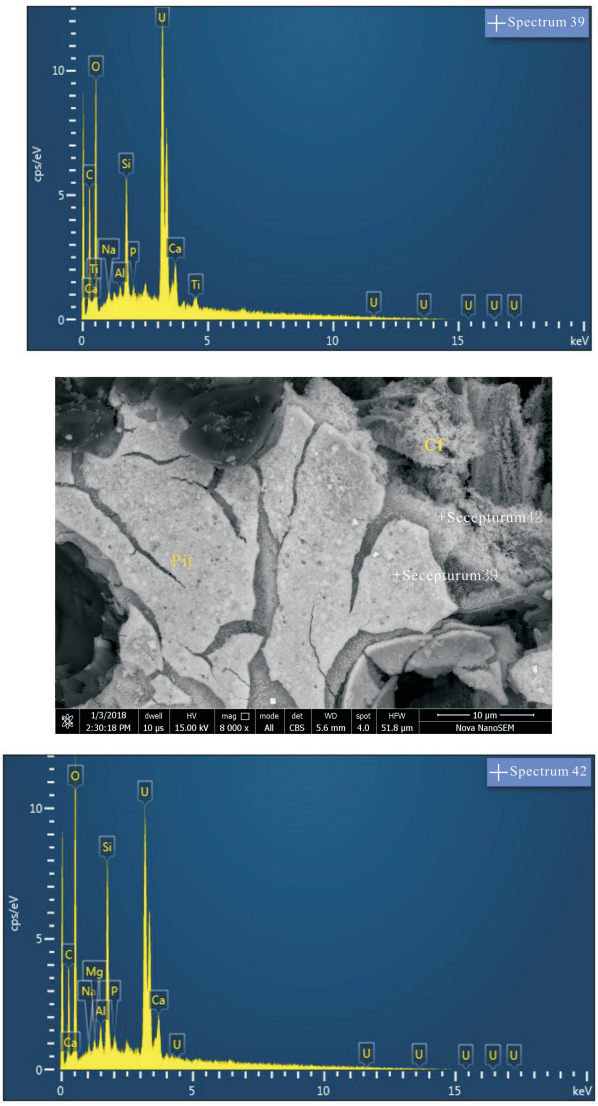


Fig. 10. Pitchblende occurring together with coffinite, Liwaxia Formation (at 80.4m depth of drill hole ZKS1–2).

4.6 Associated elements

Trace elements of sandstone from the Madongshan and Liwaxia formations were analyzed in this study. We found that after being normalized to the primitive mantle (Sun, 1989), the distribution patterns of the trace elements are similar in both formations. U, Cu, lithophile elements (such as Sr) and sulfophile elements (such as Pb) are enriched in the sandstone, but HFS elements (such as Zr, Hf, and Nb) are depleted (Fig. 13). The significant enrichment of U in the non–mineralized sandstone (Fig. 13a–b) indicates that the pre–concentration of uranium occurred as early as the diagenetic period of the ore–hosting sandstone. The pre–concentrated uranium was an abundant source for the later uranium metallogenesis in the basin. Cu is enriched in the Liwaxia Formation (Fig. 13b, d), unlike in the Madongshan Formation. On the one hand, the enriched Cu is closely related to the Cu–rich Guanshan granite in the erosion source area in the southwestern Ordos Basin, But on the other, it is also closely related to the concentrations of chalcopyrite that occurred later in the Liwaxia Formation.

Mo, V, W, Co, Ni and Mn are associated elements in the uranium ores of the Madongshan Formation, V and Co content being particularly high (Chen et al., 2011). In addition, V, Co, Ni, Mo, Cu and Pb are associated elements in the uranium ores in the Liwaxia Formation, and V, Cu and Ni content is particularly high (see Appendix Table 1). In summary, the associated elements are V, Co, Ni and Mo in the uranium target layers of the Liupanshan Group in the southern Ordos Basin, a combination of these elements being a favorable indicator in uranium prospecting.

5 Discussion

The characteristics of sandstone–hosted uranium deposits depend on the geological conditions of metallogenesis and mineralization. These conditions take into account uranium sources, structures, the lithology and lithofacies of the target layers, epigenic alterations, hydrogeology, the paleoclimate, and so forth.

5.1 Uranium sources

There are two sources of uranium in the southwestern

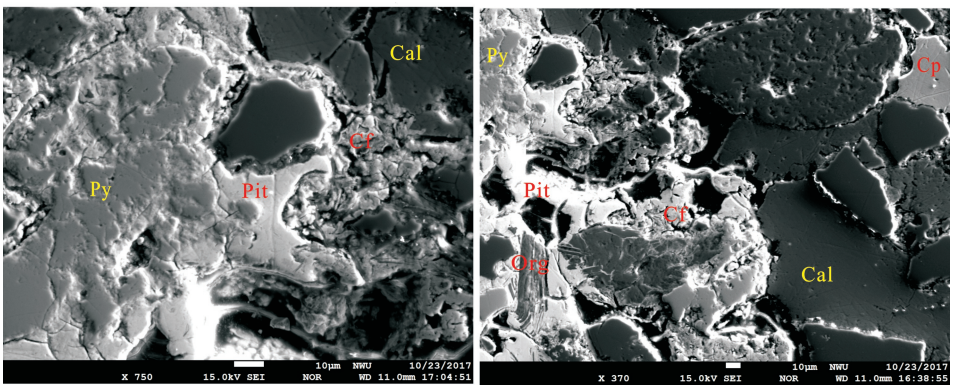


Fig. 11. The spatial relationship between uranium minerals and associated minerals.
Org– organic matter; Py– pyrite; Pit– pitchblende; Cf– coffinite; Cal– calcite; Cp– chalcopyrite

Ordos Basin: the erosion source areas and the initial sandstone of the present ore-hosting target layers. The erosion source areas in the southwestern Ordos Basin are underlain by a U-rich Proterozoic metamorphic series, uranium-bearing Indochinian granites, and U–rich Guanshan granite. Uranium content ranges from 6.2 to 15.60 ppm in the aforementioned source rocks and from 4.1 to 11.1 ppm (Lu et al., 2013) in the Lower Cretaceous sandstone. We found that uranium content in the primary sandstone of the Madongshan and Liwaxia formations in the Lower Cretaceous Series ranges from 6.25 to 15.30 ppm and from 5.29 to 11.50 ppm (see Appendix Table 1), respectively. Clearly, the present ore–hosting sandstone layer was initially a uranium–bearing formation.

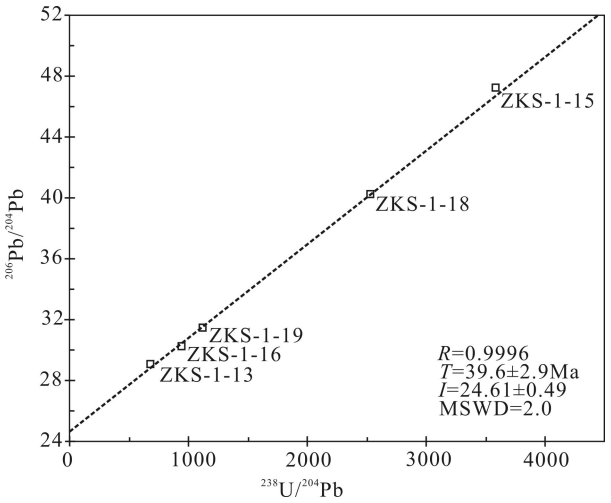


Fig. 12. The whole–rock isochronic U–Pb isotopic age of the Liwaxia Formation, Lower Cretaceous.

5.2 Structures

A tectonic slope belt that is 30–40 km long and dips at 5°–10° occurs in the bedrock of the southwestern Ordos Basin. The slope belt is a favorable tectonic setting for interlayer oxidation-type sandstone-hosted uranium mineralization. The Lijiahe syncline occurs in the cover formations of the basin. As a result of structural uplift, the target layers in both wings of the Lijiahe syncline were exposed, five entrances of charging being formed across the Liujiahe–Shenyuhe–Wucunpu–Xinjichuan area to control the direction of uranium transportation and concentration, which is necessary for epigenetic alteration and uranium mineralization in the target layers of the Lower Cretaceous Series. Unfortunately, the major target layer in the Madongshan Formation has been lifted up so much that it has been strongly eroded along with part of the uranium ore bodies in it.

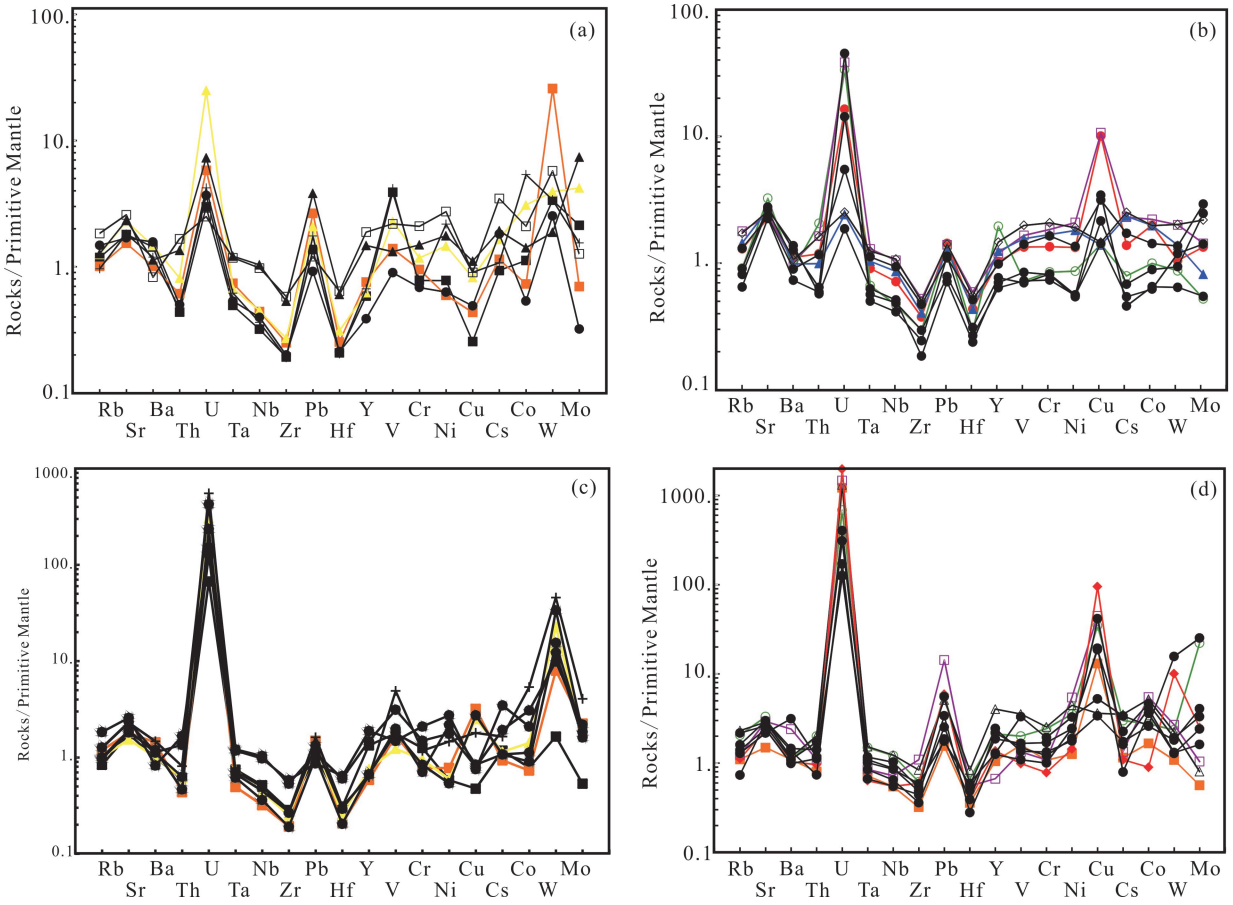


Fig. 13. Distribution curves of trace elements of the Lower Cretaceous sandstone, in the southwestern Ordos Basin (data from this paper, normalized to the primitive mantle, Sun, 1989).

(a) Non–mineralized sandstone of the Madongshan Formation; (b) Non–mineralized sandstone of the Liwaxia Formation; (c) U-ore sandstone of the Madongshan Formation; (d) U-ore sandstone of the Liwaxia Formation.

Attached list 1 Trace element analysis data of the target layers in the southwest of Ordos Basin

Classification	Sample Number	Rb	Sr	Ba	Th	U	Ta	Nb	Zr	Pb	Hf	Y	V	Cr	Ni	Cu	Cs	Co	W	Mo
No mine sandstone of Madongshan Formation	ZKG-7-1-1	92.1	216	752	4.01	6.25	0.375	3.83	37.5	24.6	1.14	10.5	233	30.4	13.2	3.83	4.01	8.96	3.7	1.15
	ZKG-7-1-3	78.5	184	528	5.61	12.2	0.561	5.29	48.7	47.7	1.39	13.6	83.3	37	10.1	6.52	4.91	5.84	28.4	0.376
	ZKG-7-1-5	97.6	275	772	7.46	52.3	0.511	5.38	52.8	37.5	1.71	11.2	137	45.7	24.8	12.3	7.07	24.6	4.32	2.27
	ZKG-7-1-6	74.9	218	624	4.28	8.83	0.469	4.34	37	31.5	1.12	12	249	27.6	37	13.5	4.62	43	3.73	0.834
	ZKG-7-1-10	115	203	824	4.6	7.7	0.405	4.76	38.9	16.5	1.17	6.96	53.8	26.7	10.7	7.33	7.8	4.27	2.78	0.173
	SCZS-1	98.9	279	593	12.4	15.3	0.921	12.4	104	68.7	3.32	26.5	79	58.1	29.9	16.6	8.28	11.3	2.06	3.99
	L1-4-1	143	309	433	15.3	5.24	0.893	11.7	113	21.6	3.51	33.8	131	81.6	46.4	13.5	14.9	16.7	6.32	0.682
No mine sandstone of Liwaxia Formation	ZKS159-1-1	101	270	583	10.9	34.4	0.689	8.58	73.3	25.7	2.39	18.5	80.3	52.5	22.6	151	5.94	15.9	1.15	0.723
	ZKS92-1-2	71	389	474	18.9	70.5	0.504	5.63	57.6	24.7	1.62	35.1	43.5	33.1	14.7	21.1	3.4	7.96	0.957	0.282
	ZKS190-1-2	75.3	278	466	8.42	25.4	0.619	8.37	80.8	13.3	2.27	17.7	65.3	49.3	14.8	7.3	4.14	8.07	0.938	0.389
	ZKS208-1-2	139	288	532	15	80.6	0.982	12.6	102	25.1	3.25	21.5	99.3	72	35.5	160	9.92	17.7	2.2	0.772
	ZKM0-1-2	112	317	517	9.13	5.07	0.786	10.3	78.6	23.3	2.38	22.3	93.5	65.7	30.8	20.8	10.1	15.8	1.52	0.44
	ZKS11-1-1	57.4	327	2655	6	34.2	0.54	6.56	58.9	16.7	1.81	14.8	49.4	35.5	11.2	22.2	2.75	5.01	1.29	0.299
	ZKS101-1-3	134	309	559	14.9	5.29	0.945	12.9	97.7	25.4	3.03	26.3	119	81.1	32.4	21.9	10.8	15.8	2.22	1.18
	ZKS57-1-1	64.1	263	473	7.1	50	0.384	4.58	46.7	17.4	1.48	16.7	36.6	26.8	12.7	64.5	2.73	7.8	1.16	0.143
	ZKS36-1-1	102	280	471	10.7	11.5	0.85	11.2	91.9	19.8	2.83	17.7	84.4	63.9	23	47.1	7.38	11.4	1.5	1.58
	ZKS236-1-1	50.5	270	384	5.43	30	0.43	5.83	57.5	14.1	1.71	13.8	41.9	32	9.55	51.6	1.97	5.21	0.708	0.295
	ZKS91-1-1	70.5	332	664	5.91	94.8	0.381	4.95	47.6	20.4	1.47	11.5	43.4	28.7	9.43	21.4	2.33	4.98	1.31	0.762
	ZKS130-1-1	63.4	318	721	5.27	3.92	0.477	6.14	36	12.8	1.31	12.6	50.7	31.7	9.23	32.2	2.93	7.11	1.03	1.33
Mineral bearing sandstone of Madongshan Formation	ZKG-7-1-2	106	167	664	3.92	156	0.578	4.86	43.7	18.4	1.31	13.9	37.8	24	7.12	2.72	6.33	4.67	1.55	0.413
	ZKG-7-1-8	65.2	210	520	5.62	141	0.567	6.16	55.3	18.9	1.69	24	106	48.7	9.85	7.1	5.05	6.29	1.81	0.288
	ZKG7-1-02	92.1	216	752	4.01	419	0.375	3.83	37.5	26.8	1.14	10.5	101	30.4	13.2	47.9	4.01	5.84	8.76	1.21
	ZKG7-1-08	78.5	184	528	5.61	636	0.561	5.29	48.7	23.3	1.39	13.6	73.7	37	10.1	37.4	4.91	11.3	25.05	0.99
	ZKG7-1-15	97.6	275	772	7.46	1160	0.511	5.38	52.8	29.1	1.71	11.2	294	45.7	24.8	27.0	7.07	43	50.3	2.19
	ZKG7-1-18	74.9	218	624	4.28	491	0.469	4.34	37	17.9	1.12	12	119	27.6	37	12.6	4.62	8.96	36.9	1.00
	ZKG9-1-02	98.7	227	710	7.14	427	0.71	8.21	68.9	28.8	2.14	8.61	54.9	42.6	6.3	9.2	8.96	3.43	5.145	0.84
	ER16-7	77.8	228	586	5.79	269	0.54	5.96	51.9	23.8	1.61	12	108.0	32.7	9.12	41.0	4.61	7.24	16.94	0.98
	ZKG7-1-01	115	203	824	4.6	202	0.405	4.76	38.9	22.3	1.17	6.96	98.0	26.7	10.7	39.7	7.8	4.27	6.41	0.9
	ZKG7-1-10	98.9	279	593	12.4	892	0.921	12.4	104	20.1	3.32	26.5	187.0	58.1	29.9	11.9	8.28	24.6	10.86	1.18
	ZKG7-1-11	143	309	433	15.3	318	0.893	11.7	113	15.6	3.51	33.8	89.0	81.6	46.4	11.3	14.9	16.7	13.44	0.87
Mineral bearing sandstone of Liwaxia Formation	HMPN-5	69.6	349	2143	4.82	150	0.331	3.79	94.1	53	1.78	41.7	50.9	23	17.6	862	2.78	10	1.19	0.186
	ZKS19-1-4	160	397	565	18.4	1433	1.13	14.5	120	100	3.67	38.3	120	94.5	60	520	12.9	22	2.59	11.9
	ZKS73-1-1	85.8	179	575	7.39	2558	0.545	6.56	62.5	27.9	1.97	18.9	95.4	42	21.4	196	4.94	13.3	1.19	0.304
	ZKS190-1-1	95.7	350	1260	10.1	3083	0.645	8.66	213	257	3.04	12	79.8	42.3	92.1	669	5.75	43.9	2.95	0.561
	ZKS190-1-5	71.1	276	519	6.38	374	0.459	5.4	72.6	163	1.85	11.3	41.7	27.2	20.6	46.9	2.57	9.82	0.784	0.438
	ZKS190-1-6	180	345	613	18.5	2756	1.16	14.7	163	91.9	4.57	72.5	213	99.2	75.5	54.3	15.1	41.5	2.46	0.433
	ZKS208-1-3	80.2	236	561	5.48	159	0.443	5.84	55	15.2	1.61	7.53	46.5	28.5	8.2	32.9	3.17	4.41	0.817	0.468
	ZKS208-1-4	87.1	283	544	8.83	4131	0.483	6.6	116	106	2.13	24.6	59.2	30.5	24.4	1420	4.68	7.17	11	1.35
	ZKS208-1-5	169	315	574	15.8	647	0.888	12.3	103	100	3.26	23.2	199	75.5	55.7	78.6	14.5	21.1	17.2	13.6
	ZKS130-1-2	70.1	339	489	9.89	111	0.747	10.5	111	20.1	3.21	18.5	85.7	55.6	21.5	79.9	3.93	14.1	1.63	1.39
	L1-13-1	57.2	344	711	6.79	357	0.505	6.58	86.2	60.9	1.53	22.5	65.3	39.1	41.6	290	3.41	28.8	1.41	1.3
	ZKM0-1-1	41.8	342	389	3.99	136	0.293	3.63	78.3	18.7	1.48	11.7	25.7	19.3	12.4	910	1.67	5.17	2.26	0.579
	ZKM0-1-3	77.9	338	561	6.99	210	0.681	5.4	62.1	20.5	1.64	12	62.1	33.6	14.3	218	4.35	9.82	1.21	1.56
	ZKS183-1-1	60.3	305	503	6.04	291	0.461	5.78	70	61.8	1.94	13.4	41.1	28.5	10.3	34.3	2.29	6.52	1.35	0.519
	ZKS183-1-2	72.7	322	738	5.68	361	0.37	4.44	50.1	25.8	1.42	12.7	39.2	25.3	11.9	89.4	2.85	7.36	0.889	0.367
	ZKS92-1-1	79.1	588	471	19.4	221	0.528	6.52	88.3	37.4	2.08	58	57.4	38.8	25.9	27.1	4.7	18.2	2.01	0.542
	ZKS157-1-2	109	288	519	10.3	265	0.64	7.76	70.1	33.4	2.15	39.4	89.4	47.3	32	50.7	7.48	20.7	1.99	2.19
	ZKS101-1-1	87.8	246	458	11.4	303	1.15	12.7	113	50.6	3.44	23.8	70	54.6	23.7	440	5.72	11.5	2.25	0.562
	ZKS101-1-2	125	357	765	13	846	0.828	10.5	94.2	45.3	2.69	33.7	99.8	66.2	41.3	280	9.72	37	2.11	1.79
	ZKS224-1-1	123	265	519	10.8	742	0.778	9.87	88.5	72.5	2.61	23.9	84.2	57.4	28.2	299	8.4	14.3	2.39	1
	L1-14-3	89.9	272	515	13.3	175	0.721	9.76	165	135	3.22	52.2	76.8	56.3	23.8	505	6.96	23.8	1.77	1.67
	L1-15-3	100	260	1646	10.8	260	0.768	10.2	114	31.7	3.11	43.9	81.3	51.9	30.1	622	6.94	32.6	1.44	0.872
	XZ-1	73.9	191	567	6.35	106	0.498	6.43	152	34.3	3.11	33	79.1	44.1	13.2	214	4.85	29.3	1.46	0.282

5.3 Lithology and lithofacies

The target layer is a sedimentary formation of red clastic rocks interlayered with gray clastic rocks. On the top section of the sedimentary formation, thick mudstones occur in the Naijiahe Formation. In the middle section, sandstones of braided stream facies occur in the Madongshan Formation and 20–40 m thick sandstones provide both pathways for uranium and hosting spaces for uranium mineralization. In the lower section, delta plain facies sedimentation, in which sandstones are interbedded with mudstones, occurs in the Liwaxia Formation. A single sandstone bed in the branch channel is 1–2 m thick. The Liwaxia Formation thus provides both some hosting space and a water-resistant bottom layer for uranium mineralization. The stratigraphic structure of the Lower Cretaceous Series is overall a mudstone–sandstone–mudstone structure, which is favorable for uranium metallogenesis in the region. Unfortunately, most sandstones in the Madongshan Formation have been lifted up by structures and eroded out; the sandstones are not well-developed in the Liwaxia Formation and are mainly fine sandstones or siltstones, both of which restrict the size of uranium deposits.

5.4 Alteration

The sandstones of the target layers in the Liupanshan Group underwent a pre–concentration of uranium in the earlier synsedimentary period, as well as reworking by phreatic oxidation, interlayer oxidation, and oil–gas reduction in the middle and later periods. As a result, phreatic oxidation zones and interlayer oxidation zones occur widely in the region, uranium mineralization that formed in later periods is superposed and reworked into earlier formations. Interlayer oxidation occurred in the Madongshan Formation and resulted in roll–shaped uranium ore bodies. Phreatic oxidation occurred in the Liwaxia Formation, where the Madongshan Formation eroded and led to the formation of lentoid or tabular uranium ore bodies.

According to analyses of sulfur isotopes, the pyrites and the chalcopyrites are clearly different in origin. The sulfur isotopic composition of the pyrites is similar to that of pyrites from the Baolongshan uranium deposit in the Songliao Basin (Xu, et al., 2011) and the Bayinwula uranium deposit in the Erlian Basin (Bonnetti, et al., 2015), which implies a biogenetic origin for the pyrites. However, the sulfur isotopic composition of the chalcopyrites (average $\delta^{34}S$ = 7.1‰) suggests that the chalcopyrites might come from depth or that the sulfur isotopes might have differentiated at depth in the fluid during chalcopyrite formation. Moreover, according to fluid inclusion analyses, the mineralization fluid in the Lower Cretaceous Series contains a little methane and is of medium–low temperature. Given that chalcopyrites occur widely in all kinds of rocks in the Liwaxia Formation, it can be further concluded that the hydrothermal fluid probably played a role in the later reductive transformation of the target layers.

According to the isochronic U–Pb isotopic ages, uranium mineralization in the study area mainly took place in the early Late Cretaceous Epoch and in the Eocene, when tectonic compression resulted in tectonic thermal events (Qu et al., 2003; Wan et al., 2005; Ren et al., 2006; Li, et al., 2008; Zhao et al., 2009; Yu, 2009). The tectonic thermal events are also consistent with the time when hydrocarbons escaped in a large quantity from the Mesozoic source rocks of the Ordos Basin (He, 2003). These thermal events might have promoted the formation and escape of oil and gas from the source rocks, which, on the one hand, provided a favorable reductive medium for uranium and, on the other hand, dissolved the oil and gas in the heated aquifer as a low–temperature hydrothermal fluid. This led to alteration in the surrounding rocks, providing a medium of remobilization and migration for uranium and accelerating the leaching of uranium out of the surrounding rocks at depth to the reducing environment, where it was concentrated to form a uranium deposit. Because oil and gas have been discovered in the target layers in the Lower Cretaceous Series (Table 4), the medium–late stage uranium mineralization may be related to the reduction of oil-gas or biological activity in the southwestern Ordos Basin (Cai et al., 2007a, b; Zhao et al., 2018).

5.5 Integrated analysis and discussion of uranium mineralization

Uranium was pre–concentrated in the red clastic formations in the southwestern Ordos Basin, which prepared a favorable source of uranium. The Lijiahe syncline and the wide–smooth slope belts on both wings of the syncline are favorable structures for uranium mineralization. The Madongshan Formation of the Lower Cretaceous contains stable sandstones from a braided stream system, is overlain by mudstone at the bottom of the Naijiahe Formation and overlies mudstone on top of the Liwaxia Formation. Such a mudstone–sandstone–mudstone stratigraphic structure both serves as a favorable structure for interlayer oxidation and also provides a hosting space for uranium concentration. Oil and gas supply the reductive medium for uranium mineralization. Hydrothermal activity helps in the superposition and enrichment of uranium. In summary, the key conditions

Table 4 The acid-split hydrocarbon and the intensity of ultraviolet fluorescence in the Lower Cretaceous interlayer oxidation zone in the southwestern Ordos Basin

Alteration zone types	Drill hole No.	Sample No.	Content of acid-split hydrocarbon			Intensity of ultraviolet fluorescence								
			Total–hydrocarbon (μL/kg)	Wet–hydrocarbon (μL/kg)	Wet–hydrocarbon / Total–hydrocarbon	320 (nm)	360 (nm)	405 (nm)	215 (nm)	220 (nm)	228 (nm)	254 (nm)	260 (nm)	280 (nm)
Oxidation zone	ZKM20-4	2	6716.65	2010.57	0.30	5.76	3.26	1.53	381.32	252.77	154.93	64.14	60.27	54.09
Transition zone	ZKM20-3	2	2350.21	765.11	0.33	18.76	14.96	3.88	403.00	272.50	168.50	73.00	66.50	54.00
Reduction zone	ZKM20-5	1	1623.06	459.66	0.28	42.08	30.24	3.88	416.00	295.00	196.00	71.00	63.00	48.00

Notes: Analytical data are obtained from the No.203 Research Institute of the CNNC

for uranium metallogenesis in the southwestern Ordos Basin include sufficient uranium sources, favorable controlling sedimentary facies and sufficient hosting space, a mudstone–sandstone–mudstone stratigraphic structure in the target layers, a structural slope belt that is favorable for interlayer oxidation (Zhang et al., 2018) and multiple stages of oxidation–reduction–reoxidation mineralization superposed on the slope belt. The aforementioned conditions, coupled together, similar to the uranium mineralization in the NW Jungar Basin (Qin et al., 2018), result in concentrations of uranium and the formation of uranium deposits in an area rich in organic matter.

The description 'five multiples but one low' characterizes uranium mineralization in the southwestern Ordos Basin according to integrated analyses of uranium geological conditions and mineralization. The Madongshan, Liwaxia and Heshapu formations in the Lower Cretaceous all have such characteristics. There are multiple prospective target layers in each formation. Uranium mineralization involves not only regional interlayer oxidation and synsedimentation mechanisms but also phreatic oxidation, infiltration and oil–gas reductive forms, possibly even superposed with hydrothermal types. The ore bodies are shaped as typical rolls, discontinuous thin slates or thin lenses. The uranium occurs predominantly in uranium minerals or more rarely is adsorbed by clays or interclay organics. The uranium minerals are mainly pitchblende and coffinite and secondarily torbernite, carnotite, uranophane, uranopilite or bayleyite. U is associated with high Cu and Ba and fairly high Mo, V, Se, Co, Ni and Mn. Organic materials are a minor component in the target layers of the Lower Cretaceous in the study area. Carbon fragments are barely visible to the naked eye in drill hole cores, and the organic content of each reduction/oxidation zone ranges from 0.01% to 0.05%. The low organic content is unfavorable for uranium mineralization.

Thus, the basic geological conditions for uranium mineralization exist in the study area; however, the 'five multiples but one low' characteristics reflect the complicated geological environment and processes of uranium metallogenesis in this area. Multiple target layers occurring in one ore district means that the limited–source uranium has been distributed across these layers; as a result, the uranium ore bodies that have formed in each layer are limited in size, so uranium prospecting in this area should focus on medium–small uranium deposits. The form of uranium mineralization varies with target layer, resulting in differently-shaped uranium ore bodies. Uranium exploration should focus on interlayer oxidation in the Madongshan and Heshangpu formations, phreatic oxidation and surface infiltration in the Liwaxia Formation, and synsedimentation in the Jingchuan Formation. The low organic matter content of the target layers is not favorable for the adsorption of uranium; therefore, regionally, uranium occurs mainly in uranium minerals, with pitchblende and coffinite being significant appropriate uranium mineralization candidates in the study area.

It is recommended that future uranium prospecting in the southwestern Ordos Basin sufficiently consider the aforementioned uranium metallogenic conditions and the 'five multiples but one low' characteristics. In districts where structures such as the Lijiahe wide–smooth syncline are developed, combined analyses of uranium geological conditions and uranium mineralization, as well as superposed geochemical anomalies of combinations of Cu, Ba, Mo, V, Co and Ni, can help effectively delineate potential uranium prospects.

6 Conclusions

(1) Basic conditions for uranium mineralization exist in the southwestern Ordos Basin. The two key factors of uranium metallogenesis are the abundant twin sources of uranium and the wide–smooth syncline. The most promising uranium prospect in this region is the syncline structure, where the reduction–oxidation transition zone in the target layer is superposed with an anomalous zone of a combination of geochemical elements.

(2) The geological environment and uranium mineralization are fairly complicated in the southwestern Ordos Basin. The unique characteristics of 'five multiples and one low' include multiple target layers, multiple stages of mineralization, multiple ore body shapes, multiple kinds of uranium minerals and multiple associated elements, but low organic matter content. Regionally, uranium exploration should focus on medium–small uranium deposits, as types of uranium mineralization vary with the target layer.

(3) Uranium mainly occurs in uranium minerals dominated by coffinite and pitchblende. Coffinite occurs in the form of an individual short–columnar crystal or an assemblage of long–columnar crystals, with pitchblende occurring as an irregular colloidal covering on the surface or as fissure-fill in the clay and carbonate minerals. Where coffinite occurs together with pitchblende, it often covers the surface of the pitchblende, clearly indicating that coffinite formed later than pitchblende.

(4) Pyrites and chalcopyrites occur widely in the red clastic formations. The genesis of the chalcopyrites obviously differed from that of the pyrites since the chalcopyrites formed later than the pyrites. Based on sulfur isotopic analyses and structural hydrothermal events of the Ordos Basin during uranium mineralization, it is suggested that some deep hydrothermal fluids or oil/gas might have played a role in the uranium mineralization processes.

Acknowledgments

This paper was jointly supported by Key Factors Identification and Targets Delineation of Sandstone Type Uranium Deposits in the Southern Ordos Basin (CNNC Integrated R&D Project, Code: Geo LTD1601–3), Scientific Research in Production Project issued by the Bureau of Geology, CNNC (Code: 201902-7) and the Chinese Geological Survey project (Code: DD20190813-5).

Manuscript received Jan. 18, 2019
accepted Oct. 22, 2019

assoicate EIC: CHI Guoxiang
edited by Jeff LISTON

Reference

Bonnetti, C., Cuney, M., Michels, R., Truche, L., Malartre, F., Liu, X.D., and Yang, J.X., 2015. The multiple roles of sulfate –reducing bacteria and Fe–Ti oxides in the genesis of the Bayinwula roll front–type uranium deposit, Erlian basin, NE China. Economic Geology, 110: 1059–1081.

Bonnetti, C., Liu X.D., Yan Z.B., Cuney, M., Michels, R., Malartre, F., Mercadier, J., and Cai, J.F., 2017. Coupled uranium mineralisation and bacterial sulphate reduction for the genesis of the Baxingtu sandstone-hosted U deposit, SW Songliao Basin, NE China. Ore Geology Reviews, 82: 108–129.

Cai, C.F., Li, H.T., Qin, M.K., Luo, X.R., Wang, F.Y., and Ou, G.X., 2007a. Biogenic and petroleum–related ore–forming processes in Dongsheng uranium deposit, NW China. Ore Geology Reviews, 32: 262–274.

Cai, C.F., Dong, H.L., Li, H.T., Xiao, X.J., Ou, G.X., and Zhang, C.M., 2007b. Mineralogical and geochemical evidence for coupled bacterial uranium mineralization and hydrocarbon oxidation in the Shashagetai deposit, NW China. Chemical Geology, 236: 167–179.

Chen, D.S., Li, S.X., and Cai, Y.Q., 2003. A discussion on research situation and development direction of sandstone–type uranium deposits in the Meso–Cenozoic basin of China. Acta Sedimentologica Sinica, 21(1): 113–117 (in Chinese with English abstract).

Chen, D.S., Liu, W.S., and Jia, L.C., 2011. Paleo-climate evolution in China and its control on the metallization of sandstone type uranium deposit of Meso–Cenozoic basins. Uranium Geology, (06): 321–326+344 (in Chinese with English abstract).

Chen, Z.Y., Chen, D.S., and Gu, K.H., 2011. China's uranium deposit research evaluation: sandstone–type uranium deposit. China Nuclear Industry Geological Survey, 231–241 (in Chinese).

Deng, J., Wang, Q.F., Huang, D.H., Gao, B.F., Yang, L.Q., and Xu, H., 2005. Basement evolution of the Ordos basin and its constraint on cap rock. Earth Science Frontiers (Chinese University of Geosciences, Beijing; Peking University), (03): 91–99 (in Chinese with English abstract).

Guo, C.L., Geng, H.J., Rong, X., and Yang, K., 2015. The controlling factors and metallogenic model of the Dahong mountain uranium deposit in western Chaoshui Basin. Acta Mineralogica Sinica, (S1): 288–289 (in Chinese).

He, Z.X., Yang, H., and Fei, A.Q., 2003. Evolution and Oil Gas of Ordos Basin. Beijing: Petroleum Industry Press, 88–173 (in Chinese).

Hao, Y.C.,1986. Cretaceous of China. Beijing: Beijing Geological Publishing House, 15–32 (in Chinese).

Jiang, B.G., Shen, Z.M., Zhu, B., Sun, L.Q., and Huang, S.Q., 2017. Geological features and metallogenic model of sandstone type uranium deposit in Hengyang Basin. Uranium Geology, (02): 82–88 (in Chinese with English abstract).

Kang, S.H., 2011. The influence of sedimentary background on uranium metallogenic type in Ulanchabu depression, Erlian Basin. Progress Report on China Nuclear Science & Technology (Vol.2) Volume 1 of the 2011 Academic Year of the Chinese Nuclear Society (Uranium Geology Branch), 8 (in Chinese).

Li, C.Y., Wang, Q., Zhang, Z.M., and Liu, X.Y., 1980. A preliminary study of plate tectonics of China. Bulletin of the Chinese Academy of Geological Sciences, (00): 11–19 (in Chinese with English abstract).

Li, W.H., Zhang, S.M., Guo, C.L., and An, W.T., 2010. The characteristics of gray–white alteration of sandstone in the Hongshan uranium deposit and its prospecting significance. Mineral Deposits, (S1): 139–140 (in Chinese).

Li, X.D., Liu, J.G., and Yi, C., 2017. The genesis of uranium ore with red alterations in the Nalinggou deposit, northeastern Ordos Basin, and its geological implications. Geological Bulletin of China, 36(4): 511–519 (in Chinese with English abstract).

Li, Z.Y., Fang, X.H., Chen, A.P., Ou, G.X., Xiao, X.J., Sun, Y., Liu, C.Y., and Wang, Y., 2007. Genesis of gray green sandstone in uranium target layer in north Ordos Basin. Science China (D: Earth Science), (S1): 139–146(in Chinese).

Li, Z.Y., Chen, A.P., Fang, X.H., Ou, G.X., Xia, Y.L., and Sun, Y., 2008. Origin and superposition metallogenic model of the sandstone–type uranium deposit in the northeastern Ordos Basin, China. Acta Geologica Sinica (English Edition), 82(4): 745–749.

Liu, J.P., Xie, S.Y., Liu, K.Q., and Yuan, W.G., 1986. Evolution stacking and hydrocarbon potential of the Ordos basin: prototypel analysis of a huge basin in Chinese continental plate. Oil and Gas Geology, (04): 356–367 (in Chinese with English abstract).

Liu, X.Z., Feng, M.Y., and Luo, C.B., 1997. China's Uranium Prospecting Guide. China Nuclear Industry Geological Survey, 139–206 (in Chinese).

Lu, B.L., 2013. Metallogenic conditions and prospective prediction of uranium deposits in southern Ordos Basin. Northwest University (in Chinese with English abstract).

Lu, Y.F., 2004. GeoKit-A geochemical toolkit for Microsoft Excel. Geochimica, 033(005): 459–464.

Luo, Y., Ma, H.F., Xia, Y.L., and Zhang, Z.G., 2007. Geologic characteristics and metallogenic model of Qianjiadian uranium deposit in Songliao basin. Uranium Geology, (04): 193–200 (in Chinese with English abstract).

Norrish, K., and Hutton, J.T., 1969. An accurate X-ray spectrographic method for the analysis of a wide range of geological samples. Geochimica Et Cosmochimica Acta, 33 (4): 431–453.

Pang, Y.Q., Chen, X.L., Fang, X.H., and Sun, Y., 2010. Discussion on the interlayer oxidation and uranium metallogenesis in Qianjiadian uranium deposit, Songliao Basin. Uranium Geology, (01): 9–16+23 (in Chinese with English abstract).

Qu, H.J., Li, W.H., He, X.P., Liang, W.H., Li, R.J., and Wang, W.W., 2003. Discussion on sequence stratigraphy and petroleum system of the Lower Cretaceous in Liupanshan Basin. Journal of Northwest University (Natural Science Edition), 1(33): 70–74.

QIN, M.K., HUANG, S.H., HE, Z.B., XU, Q., SONG, J.Y., LIU, Z.Y., and GUO, Q., 2018. Evolution of Tectonic Uplift, Hydrocarbon Migration, and Uranium Mineralization in the NW Junggar Basin: An Apatite Fission-Track Thermochronology Study. Acta Geologica Sinica (English Edition), 92(5): 1901–1916

Ren, Z.L., Zhang, S., Gao, S.L., Cui, J.P., and Liu, X.S., 2006. Research on region of maturation anomaly and formation time in Ordos basin. Acta Geologica Sinica, (05): 674–684. (in Chinese with English abstract).

Song, J.J., 1993. Cretaceous system in Gansu. Acta Geological Gansu (suppl.), 1–49 (in Chinese with English abstract).

Sun, G., and Zhao, Z.H., 1998. Uranium Geology in Western–Northern Era of China. Xi'an: Northwest Geologic Bureau of CNNC, 305–318 (in Chinese).

Wan, C.L., Fu, J.H., and Zhang, J., 2005. Tectono–thermal event in west foreland basin of Ordos and its effects on oil-gas migration. Journal of Earth Sciences and Environment, 27(2): 43–47.

Xu, Z., Wu, R.G., Yu, D.G., Rao, M.H., Li, Y.L., Gao, Y.Y., and Yu, B.L., 2011. Features of hydrothermal alteration of sandstone-type uranium in Songliao Basin. Journal of East China Institute of Technology, (03): 201–208 (in Chinese with English abstract).

Yang, Y.Y., 2006. Cretaceous sedimentary formation in Ordos basin. Oil & Gas geology, (27): 167–172 (in Chinese with English abstract).

Yi, C., Gao, H.W., Li, X.D., Zhang, K., Chen, X.L., and Li, J.X., 2015. Study on indicative significance of major elements for sandstone-type uranium deposit in Zhiluo Formation in northeastern Ordos Basin. Mineral Deposits, 34(04): 801–803 (in Chinese with English abstract).

Yu, Q., 2009. The thermal evolution history of Ordos Basin Mesozoic and its relationship with various energy mineral

deposit. Northwest University, 23–47.
Zhang, J.D., Xu, G.Z., and Peng, Y.B., 2014. Uranium Geology in Northwestern China. Beijing: China Nuclear Geology, 316–321.
Zhang, L., Liu, C.Y., Fayek, M., Wu, B.L., Lei, K.Y., Cun, X.N., and Sun, L., 2017. Hydrothermal mineralization in the sandstone–hosted Hangjinqi uranium deposit, North Ordos Basin, China. Ore Geology Reviews, 80: 103–115.
Zhang, Y.Q., Shi, W., and Dong, S.W., 2011. Changes of Late Mesozoic tectonic regimes around the Ordos Basin (North China) and their geodynamic implications. Acta Geologica Sinica (English Edition), 85(6): 1254–1276.
Zhang, Z.L., Fan, H.H., He, F., Li, W.H., Li, Y.F., Yi, L.S., and Yang, M.J., 2018. Analysis of sandstone type uranium metallogenic conditions of Lower Cretaceous in the southwest margin of Ordos Basin. Uranium Geology, 34(04): 193–200 (in Chinese with English abstract).
Zhao, J.L., Tan, C.Q., and Liu, C.Y., 2009. Analysis of impact factors on the uranium enrichment and distribution in the Ordos Basin. Acta Geologica Sinica, 83(2): 158–165 (in Chinese with English abstract).
Zhao, L., Cai, C.F., Jin, R.S., Li, J.G., Li, H.L., Wei, J.L., Guo, H., and Zhang, B., 2018. Mineralogical and geochemical evidence for biogenic and petroleum–related uranium mineralization in the Qianjiadian deposit, NE China. Ore Geology Reviews, 101: 273–292.
Zhu, R.K., Cui, J.W., Deng, S.H., Luo, Z., Lu, Y.Z., and Qiu, Z., 2019. High-precision dating and geological significance of Chang 7 tuff zircon of the Triassic Yanchang Formation, Ordos Basin in Central China. Acta Geologica Sinica (English Edition), 93(6): 1823–21834.

About the first author



ZHANG Zilong, male, born in 1978 in Genhe City, Inner Mongolia; Ph.D; graduated from Beijing Research Institute of Uranium Geology; Professor of Beijing Research Institute of Uranium Geology, CNNC. He is now devoting himself to uranium exploration, sedimentology, fluid inclusion studies and other related fields. Email:ZZL99132@163.com. Phone: 010-64964237, 13717700213.

About the corresponding author



YI Longsheng, male, born in 1981 in Qixia City, Shandong Province; Ph.D; graduated from the Institute of Geology and Geophysics, University of China Academy of Science; Senior engineer of the Beijing Research Institute of Uranium Geology, CNNC. He is now devoting himself to uranium exploration, ore deposit geology, fluid inclusion studies and other related fields. Email: roedder@126.com. Phone: 010-84860305, 13810098451.